Alexandria Engineering Journal (2017) xxx, xxx–xxx

HOSTED BY

Alexandria University

Alexandria Engineering Journal

www.elsevier.com/locate/aej
www.sciencedirect.com

ORIGINAL ARTICLE

Experimental/numerical investigation of mechanical behaviour of internally pressurized cylindrical shells with external longitudinal and circumferential semi-elliptical defects

H. Moustabchir [a], J. Arbaoui [b], Zitouni Azari [c], S. Hariri [d], Catalin Iulian Pruncu [e,*]

[a] *Équipe Science et Ingénierie des Matériaux (ESIM), Département de Physique Faculté des Sciences et Techniques Errachidia, Université My Ismaïl, BP 509 Boutalamine, 52000 Errachidia, Morocco*
[b] *ENSTA-Bretagne, MSN/LBMS/DFMS, 2 rue François Verny, 29806 Brest, France*
[c] *LaBPS, Ecole Nationale d'Ingenieurs de Metz, Ile du Saulcy, 57045 Metz, France*
[d] *Département Technologie des Polymères et Composites and Ingénierie Mécanique, Ecole des Mines de Douai 941, rue Charles Bourseul, B.P. 10838, 59508 Douai Cedex, France*
[e] *School of Mechanical Engineering, University of Birmingham, Edgbaston B15 2TT, United Kingdom*

Received 11 October 2016; revised 6 April 2017; accepted 22 May 2017

KEYWORDS

Internally pressurized cylindrical shells;
Longitudinal and circumferential semi-elliptical defects;
Strain gauges;
Finite element simulations

Abstract This paper presents an experimental-numerical investigation on the mechanical behaviour of pressurized cylindrical shells with external longitudinal and circumferential cracks of semi-elliptical shape. The research is motivated by the need to develop advanced design methodologies for shell structures. For that purpose, strain gauges are utilized to monitor strain concentrations near the cracks, and finite element simulations are carried out to predict the corresponding stress intensity factor distributions. A good agreement between numerical simulations and experimental data is found. This confirms that virtual simulations/calculations provide a reliable approach to evaluating mechanical behaviour of pressurized cylindrical shells with crack defects.

1. Introduction

The growth in energy demand entails increasing size of industrial structures. Components involved in power plant, oil & gas facilities and petrochemical networks that are under mechanical pressure constitute an attractive deal for research scientists since several decades. In particular, the pipeline installations for oil and gas transmission have drastically increased in the last three decades [1–3]. Long-term exploitation of such structures facilitates their damaging [4] that can be accelerated by the external environmental conditions such as corrosion or erosion. This puts a challenge to designers: to evaluate the progress of mechanical damage. Damage processes may be activated due to accumulation of effective stress

* Corresponding author.
E-mail address: c.i.pruncu@bham.ac.uk (C.I. Pruncu).
Peer review under Responsibility of Faculty of Engineering, Alexandria University.

http://dx.doi.org/10.1016/j.aej.2017.05.022

Please cite this article in press as: H. Moustabchir et al., Experimental/numerical investigation of mechanical behaviour of internally pressurized cylindrical shells with external longitudinal and circumferential semi-elliptical defects, Alexandria Eng. J. (2017), http://dx.doi.org/10.1016/j.aej.2017.05.022

concentrators [5,6] that may cause initiation and growth of surface cracks and finally leads to catastrophic failures.

Methods for assessing mechanical failure modes of pressurized components play a critical role [7–9] in ensuring safe operation conditions of pressure vessels, piping systems and storage tanks. Structural health monitoring techniques ultimately have to evaluate the critical defect sizes that lead to select specific procedures for repairing protocols and life extension programmes to keep in-service structural components or change their critical parts. In this context, fracture mechanics based approaches provide a reliable basis to decide the type and the schedule of repairing/maintaining operations to be carried out. The correlation between crack size and applied loads is measured by a linear elastic stress intensity factor, K, or by an elasto-plastic parameter defined by the J-integral [10] and its corresponding value of the crack tip opening displacement, CTOD.

Disposing of reliable solutions based on the hoop stress calculation [11] is fundamental for circumferentially/axial cracked pipes.

Furthermore, for a given stress state, a limit load [8,12–14] can be determined and expressed in terms of local and/or global limit approaches [15,16]. For example, [17,18] embedding global limit load solutions have developed a correct procedure to evaluate the mechanical behaviour of a thick-walled cylinder with global circumferential internal and/or external and through-wall defects. Theoretical approaches were confirmed by 3D elastic-plastic finite element analyses [19].

This study will demonstrate the harmfulness of defects hosted in pipe lines under internal pressure. In particular, the effect of semi-elliptic external notches in cylindrical shells is analysed. For that purpose, experimental measurements are carried out on specimen models following the recommendations of CODAP code, accounting for the presence of circumferential and longitudinal defects. Specimens are instrumented with extensometric gauges in order to measure deformations. It comes out that the opening stress at notches is the critical parameter driving crack propagation. Experiments are then simulated by finite element models run in the Castem software environoment setting the same dimensions and crack locations observed in the tests. Results of numerical simulations are in excellent agreement with experimental observations.

2. Experimental

2.1. Determination of material properties

The structural behaviour of a cylindrical shell including longitudinal and circumferential external defects subjected to internal pressure was investigated. The chemical composition of the considered material (steel P264GH) was determined via scanning electron microscopy (SEM) and was found to be consistent with the literature (see Table 1). Mechanical properties are listed in Table 1.

Samples tested for determining mechanical properties of the P264GHs steel are shaped as standard tensile specimens, machined from cylindrical ferrule in the longitudinal direction. These tests were performed on the INSTRON 5585H machine shown in Fig. 1, equipped with a static load cell of ±250 kN and pneumatic jaws, configuration in agreement with the European standard [20]. At least four tests were carried out by pulling the specimen in the longitudinal direction. The experimental results are presented in Table 2. Standard deviations on measured properties were at most 2.73% of the corresponding average values listed in the last row of the table. The sample geometry is given in Fig. 2.

A typical stress-strain curve recorded in the tests is plotted in Fig. 3. Experimental data are very well fitted by the Ramberg-Osgood law:

$$\varepsilon = \frac{\sigma}{E} + \left(\frac{\sigma}{K}\right)^{1/n} \quad (1)$$

where $k = 494.54$ MPa; $n = 0.068$.

2.2. Tests on internally pressurized cylindrical shells

Samples are shaped as cylindrical ferrules closed by semi-spherical caps at both ends (see Fig. 4). The limit load of these structures can be determined using the analytical expressions proposed in [21–24], for structures containing notch defects, that describe the evolution of the stress near these defects.

Experimental tests on internally pressurized pipe-like specimens were carried out at the Laboratory of Mechanics School (Douai, France), considering the D construction category of the CODAP 2000 design code [25]. The main geometric dimensions of the tested specimens are shown in Fig. 5. In practical applications, this component is used for water chain. According to the CODAP standard, the nominal stress σ_n developed in the specimen is 147 MPa.

The calculation of pressure in this cylindrical ferrule is obtained by inverting the formula of the CODAP [14]

$$P = \frac{2 \times \sigma_n \times t \times z}{D_m} \quad (2)$$

where

D_m: Average diameter of the envelope,

σ_n: Nominal stress,

z: Coefficient of welding. As the ferrule is taken in tube without weld, one will take $z = 1$.

Eq. (2) gives a value of internal pressure $P = 74$ bar for the developed stress of 147 MPa.

The defects located in the external surface of tested samples were created by submitting cylindrical ferrules to electron discharge machining. In this way, specimens included circumferential and longitudinal defects of semi-elliptical shape. The configuration of defect is defined by the length of defect "2c", depth of the defect "a", 2c and tip radius of notch "ρ".

Table 1 Chemical composition of P264GH steel element weight %.

Material	C	Mn	Si	S	P	Al	Fe
Tested steel	0.123	0.665	0.195	0.002	0.013	0.027	Bal.
Steel P264GH according to standard EN 10028.2-92	0.18	1	0.4	0.015	0.025	0.02	Bal.

Please cite this article in press as: H. Moustabchir et al., Experimental/numerical investigation of mechanical behaviour of internally pressurized cylindrical shells with external longitudinal and circumferential semi-elliptical defects, Alexandria Eng. J. (2017), http://dx.doi.org/10.1016/j.aej.2017.05.022

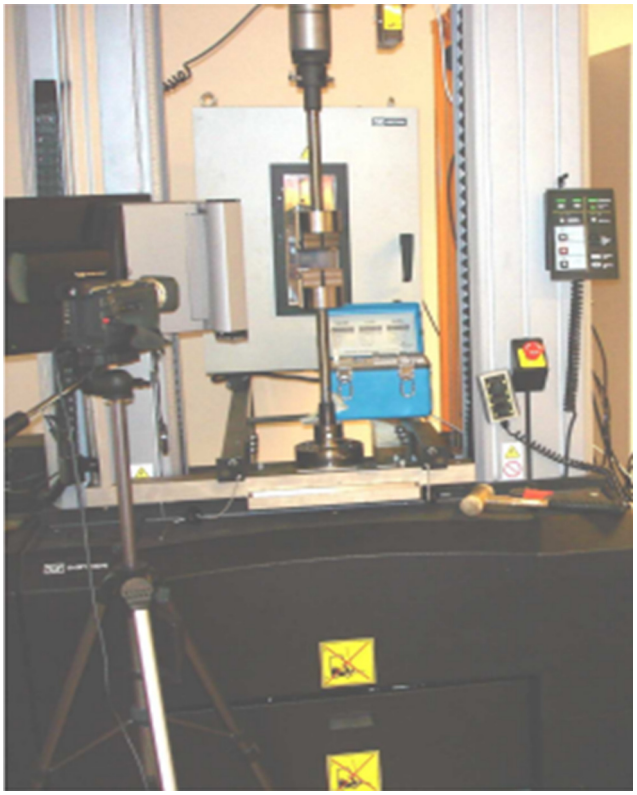

Figure 1 Experimental setup for tensile tests.

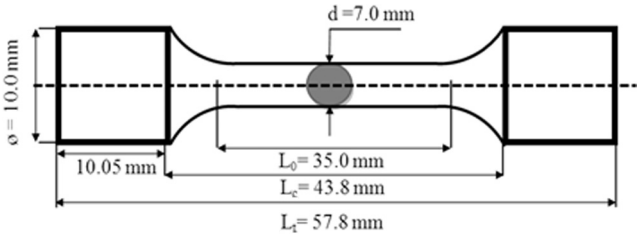

Figure 2 Geometry of tensile specimens used for determining mechanical properties of the P264GH steel.

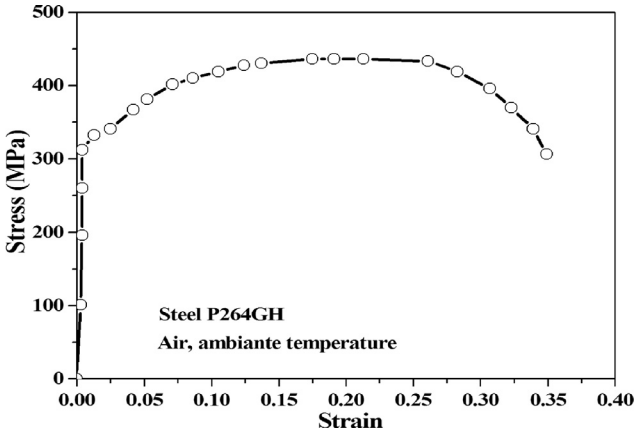

Figure 3 Typical stress-strain diagram of steel studied.

Fig. 6 shows the schematic views of two specimens including longitudinal or circumferential defects; the corresponding parameters defining defect geometry also are indicated. Table 3 reports the values of characteristic dimensions selected for each defect.

In this study, a limited number of samples were tested due to considerable specimen size. Similarly, we considered fixed geometric configurations. A more extensive campaign will be carried out in the near future to confirm experimental observations on a statistical basis.

2.3. Strain gauge set up

The extensometric device shown in Fig. 7 was used to measure the strain tensor components.

2.3.1. Working principle

Strain gages are applied on the surface of the specimen to measure changes in the length while the deformations are directly linked to the relative variation in their electrical resistance developed in the specimen compound. For a conductive wire with resistivity ρ^* (Ω m), of uniform cross-section S and length L, electrical resistance can be expressed as:

$$R^* = \frac{\rho^* L}{S} \ (\Omega) \tag{3}$$

The variation of R due to loading mechanism corresponds to the following equation:

$$\frac{\Delta R^*}{R^*} = \left[\frac{\Delta R^*}{R^*}\right]_{\varepsilon} + \left[\frac{\Delta R^*}{R^*}\right]_{\Delta\theta} \tag{4}$$

– $\left[\frac{\Delta R^*}{R^*}\right]_{\varepsilon}$: Relative change in resistance due to the deformation of the gauge,
– $\left[\frac{\Delta R^*}{R^*}\right]_{\Delta\theta}$: Relative change in resistance due to variation of temperature.

Table 2 Mechanical properties of the P264GH steel obtained in the tensile tests.

Tests	Modulus of elasticity (MPa)	Yield strength (MPa)	Poisson's ratio	Ultimate tensile strength (MPa)	Elongation to fracture
1	E = 20,7000 MPa	R_e = 340 MPa	v = 0.3	R_m = 440 MPa	A = 35%
2	E = 20,6000 MPa	R_e = 339 MPa	v = 0.29	R_m = 440 MPa	A = 34%
3	E = 20,7000 MPa	R_e = 340 MPa	v = 0.3	R_m = 440 MPa	A = 35%
4	E = 20,8000 MPa	R_e = 341 MPa	v = 0.31	R_m = 440 MPa	A = 36%
Average	E = 20,7000 MPa	R_e = 340 MPa	v = 0.3	R_m = 440 MPa	A = 35%

Please cite this article in press as: H. Moustabchir et al., Experimental/numerical investigation of mechanical behaviour of internally pressurized cylindrical shells with external longitudinal and circumferential semi-elliptical defects, Alexandria Eng. J. (2017), http://dx.doi.org/10.1016/j.aej.2017.05.022

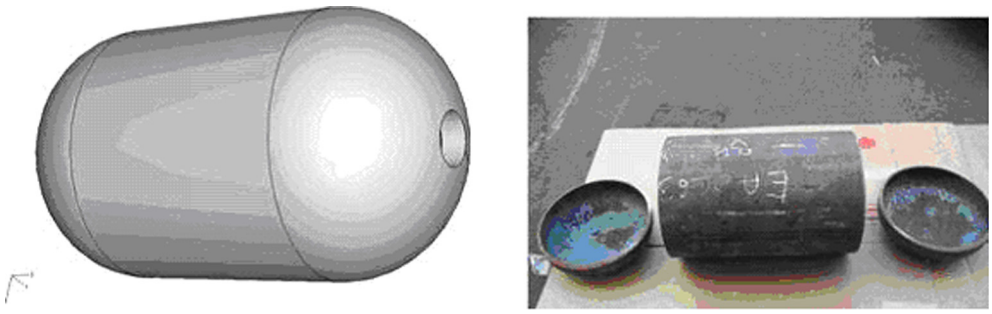

Figure 4 Typical internally pressurized specimen tested in this study.

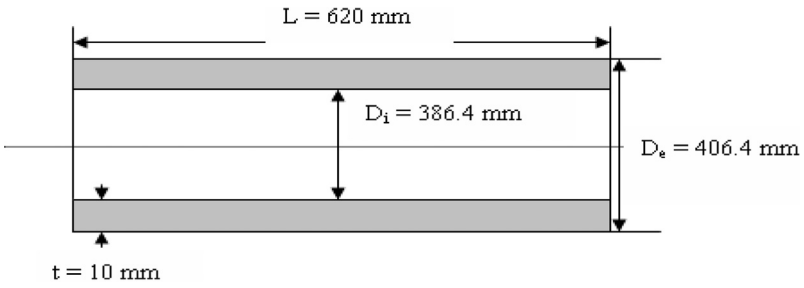

Figure 5 Nominal dimensions of the internally pressurized specimens tested in this study.

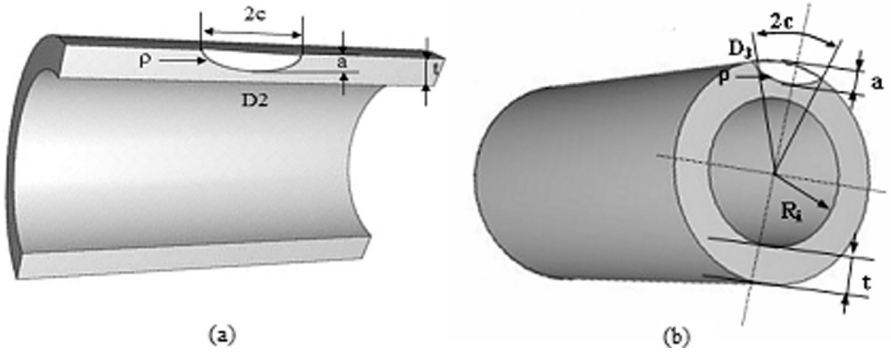

Figure 6 Position and dimensions of defects, (a) longitudinal and (b) circumferential.

Table 3 Geometric dimensions of external semi-elliptical defects.

Defect's number	Location	Size (mm)		
		a	c	ρ
D_2	Axial	2	8	0.25
D_3	Circumferential	2	8	0.25

At constant temperature,

$$\frac{\Delta R^*}{R^*} = \left[\frac{\Delta R^*}{R^*}\right]_{\varepsilon} = \frac{\Delta \rho^*}{\rho^*} + \frac{\Delta L}{L} - \frac{\Delta S}{S} \tag{5}$$

Each change length ΔL corresponds to a modified value in the electrical resistance of the gauge ΔR^* measured by a Wheatstone bridge.

$$\frac{\Delta R^*}{R^*} = [(1+2v) + c(1-2v)]\frac{\Delta L}{L} \tag{6}$$

$$\frac{\Delta R^*}{R^*} = k\frac{\Delta L}{L} \tag{7}$$

Here, k is the gauge factor which depends on the material properties, v the Poisson's ratio of the material and c the Bridgman constant.

An ideal strain gauge needs to be perfectly glued on the structure under study because it could be very sensitive to any deformations thereof. It consists of a wire (generally Constantan material) bonded in a close winding structure, guided into a thin carrier. The final shape of the gauge, containing a film frame, is obtained from a thin metal sheet (a few μm thick) and an insulating support (a synthetic resin).

Here, we used a simple chain structure composed of several equidistant gauges covering an area of 2 mm^2. Measurements are performed using conventional Wheatstone bridges with a fourth mounting bridge where the signal data is transmitted to a central automatic acquisition, which allows the acquisition, storage and processing of data.

Please cite this article in press as: H. Moustabchir et al., Experimental/numerical investigation of mechanical behaviour of internally pressurized cylindrical shells with external longitudinal and circumferential semi-elliptical defects, Alexandria Eng. J. (2017), http://dx.doi.org/10.1016/j.aej.2017.05.022

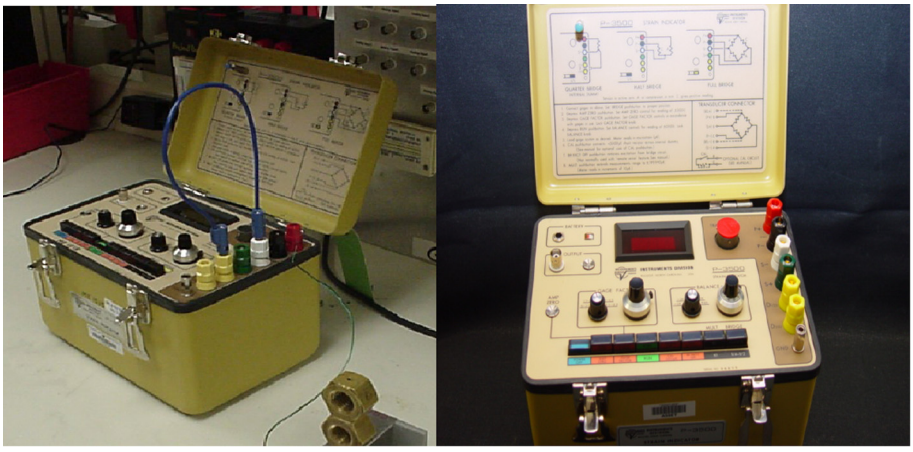

Figure 7 Extensometric bridge used in the experiments on pressurized vessel like specimens.

A total of 35 gauges elements were utilized in order to accurately detect the deformation field of the tested specimens. Fig. 8 shows the strain gauge arrangement for two specimens containing an axial defect D2 and a circumferential defect D3, respectively. The gauges installed near defects allow to obtain pressure-deformation curves.

2.4. Experimental results

Deformations of regions near defects were inspected with strain gauges. For that purpose, 4 chains of 5 gauges were applied to the specimen surface as it is shown in the schematics of Fig. 9. This arrangement allows to accurately detect strain concentrations caused by the presence of defects.

The instrumented specimens were loaded by internal pressure in order to detect evolution of deformations in the regions near defects. The effect of the presence of semi-elliptical defects in the longitudinal direction was studied also in [25] but with an experimental setup less sensitive to deformation gradients in the vicinity of the defect. Nevertheless, the defect was clearly identified as the cause of crack initiation and propagation. Here, specimens were loaded by internal pressure p and the circumferential deformation $\varepsilon_{\theta\theta}$ was measured near the defect. Fig. 10 shows the evolution of the pressure (in bar) with respect to the circumferential deformation $\varepsilon_{\theta\theta}$ recorded by the J_1 gauge of the C_4 chain located at 2 mm of the edge of longitudinal defect D_2 and the same deformation recorded by gauge J2 placed at 2 mm from J1.

The results in terms of pressure vs deformations show a linear behaviour on the initial state of material loading that represents the 0.2% plastic strain limit. The strain gauge layout illustrated by Fig. 9 allows to monitor circumferential deformations that develop at the point J1 where stresses are maximal because the crack front is close to J1. As far we move away from J1, in the vicinity of J2, deformations start decreasing and stresses drop down even if material behaviour remains in the elastic domain. Near defect D3, it was observed an increase in longitudinal deformation up to a plateau value (see discussion in Section 3.2).

Obviously, different material behaviour was observed in correspondence of strain gauges J1 and J2: the load path (e.g. applied internal pressure vs. circumferential deformation) became nonlinear at, respectively, 1111.7 με and 766.9 με which corresponds to pressure levels of 40 bar for J1 and 43 bar for J2. This suggests that local plasticization occurs near the defect caused by stress concentrations softening the material at different extents.

3. Numerical simulation

The experimental tests carried out in this study were simulated by a finite element model in order to perform a parametric analysis. The FE model included an adaptive meshing properly refined near the defect and special elements at the bottom of the notch around the surface of discontinuity [18]. The level of applied pressure was limited to 25 bar in order to remain

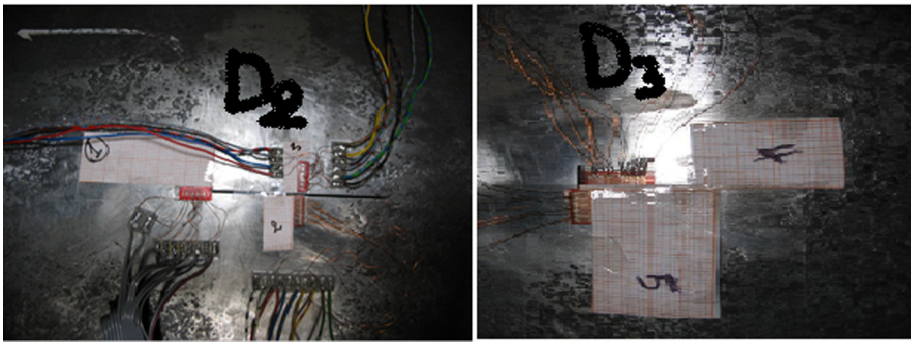

Figure 8 Assembly view of tested specimens with strain gauges applied near defects.

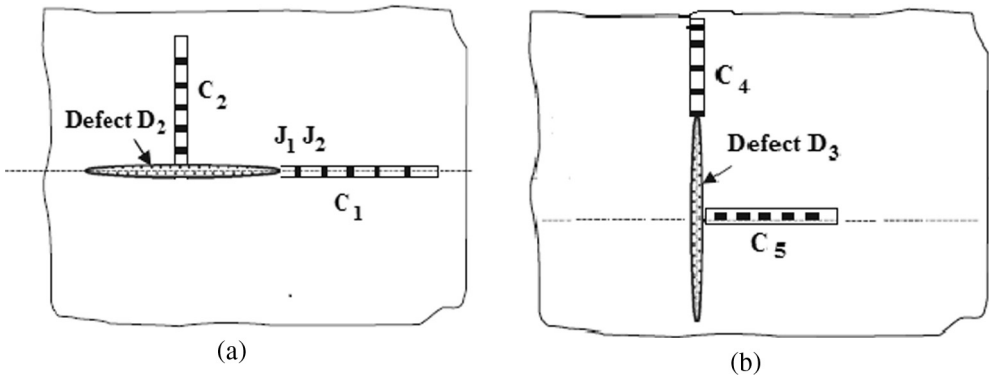

Figure 9 Schematic of strain gauge locations for measuring deformation near (a) longitudinal defect D2 and (b) circumferential defect D3.

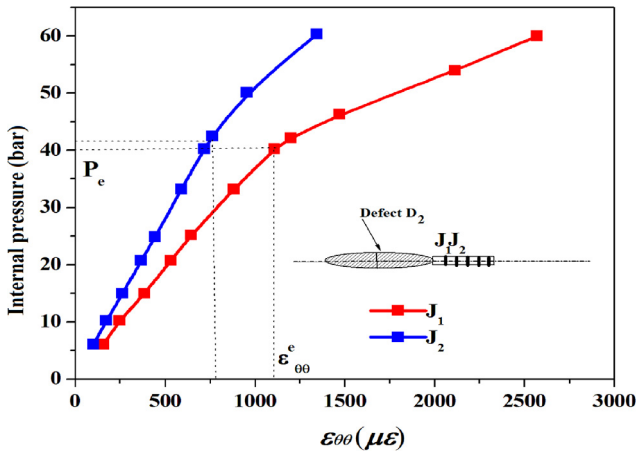

Figure 10 Variation of applied internal pressure vs. circumferential deformation near the tip of the longitudinal defect.

in the linear elastic regime. This limitation agrees with experimental observations (see Fig. 10), because the applied pressure produces effects only in the elastic behaviour, that is far enough to avoid the initiation of plastic deformations mechanisms.

3.1. Finite element modelling

The type I waste tank (386.4 mm in internal diameter, 620 mm in length, and 10 mm in wall thickness, i.e. having the main dimension cited in Fig. 6) was used as a typical geometry in the numerical analyses. A through-wall axial crack was assumed to exist in the mid-tank location.

Because of symmetry [26,27], only a quarter of the tank was modelled as shown in Fig. 11. The mesh, comprised of quadratic hexahedral elements with 20 nodes (CU20), was refined near crack boundaries. The typical model in Fig. 11 contains 67425 elements and 73088 nodes. Proper boundary conditions (bindings) were chosen to verify the symmetry assumption. Since accuracy of FE solutions depends on the element type and the level of mesh refinement near the crack tip, dedicated self-meshing cracking tools were utilized.

This adaptive self-meshing cracking technique was build using pentahedron elements of Barsoum, starting from a Serendip element H20 [28] as follows:

- The nodes located on the crack front perpendicular to the edges are placed at quarter of the edge and not in the middle, which indicates the correct asymptotic behaviour for the displacement field,
- The edge located on the crack front, created from the degeneration of a face hexahedron H20, permits obtaining a bounded integral. The stiffness matrix associated with the new element may then be evaluated by a conventional point rule of Gaussian quadrature. A graphical procedure is represented in Fig. 12.

This technique causes the creation of a tubular mesh centred on the crack front and composed of Barsoum elements. Usually the first ring is extruded on several levels so as to obtain a mapped mesh in a tubular neighbourhood of the crack tip, crack-called block (BF). The secondary crowns are discretized using H20 standard elements, allowing to properly represent the stress gradients in an extended neighbourhood of the crack front. Since hexahedral elements have a higher rate

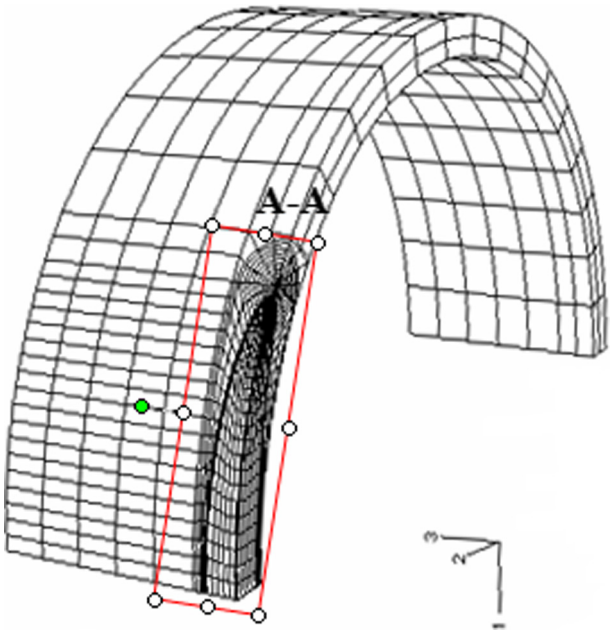

Figure 11 Finite element mesh for a quarter of a notched pipe with an external surface crack.

of convergence than tetrahedral elements, it is necessary to radiate the hexahedral mesh as much as possible in the radial direction at the crack tip so as to obtain an optimum model.

3.2. Comparison of FE simulations and experimental data

The FE models developed in this study include different orientations of defects D2 and D3, according to Fig. 6 and Table 3. The model was parametrized so as to cover all defect geometries considered in the experiments with a/t, t/Ri, c/a and $\rho = 0.25$ mm [29]. Fig. 13 compares the FE results with the experimental data gathered for the shells with the longitudinal defect D2 tested at the internal pressure of 25 bar. Besides the excellent agreement between experimental results and FE simulations, it can be seen that the circumferential strain increases up to an asymptotic value which is reached at a distance of 7 mm from the defect. The region located between 2 and 7 mm from the defect hosts strain concentration while the region located between 7 and 10 mm from the defect is not affected by the presence of the defect itself. As a counterpart, Fig. 14 shows that the longitudinal deformation gradually decreases and then stabilizes as we move away from the tip of defect D2. Experimental results and FE simulations again agree very well. From Figs. 13 and 14, it appears that circumferential strain is three times as large as longitudinal strain. Numerical and experimental results obtained for the shells including circumferential defects D3 also agree very well. It can be seen that the circumferential deformation is almost constant along the direction of the defect (Fig. 15): this proves that crack propagation is not affected by the presence of circumferential defects. Conversely, longitudinal strain increases up to an asymptotic value (Fig. 16) which is however almost four times lower than circumferential strain. The present study confirmed that longitudinal defects are more dangerous than circumferential defects in terms of crack propagation for cylindrical shells loaded by internal pressure. The longitudinal strain that may cause the propagation of a circumferential defect is very low compared to the circumferential strain that may favour the opening of a longitudinal defect. If a pressurized cylindrical shell includes both longitudinal and circumferential defects of the same size, the former will cause initiation and propagation of the crack/cracks.

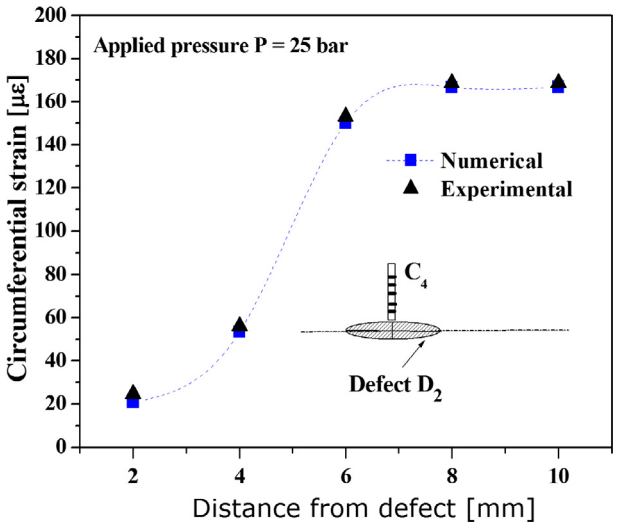

Figure 13 Distribution of circumferential strain near defect D_2.

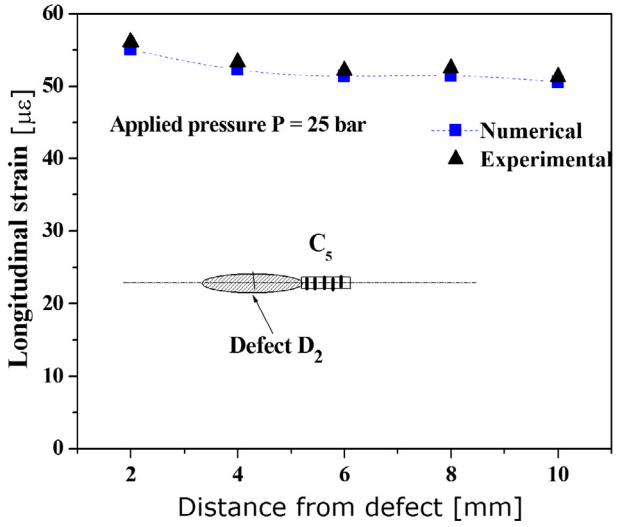

Figure 14 Distribution of longitudinal strain near defect D_2.

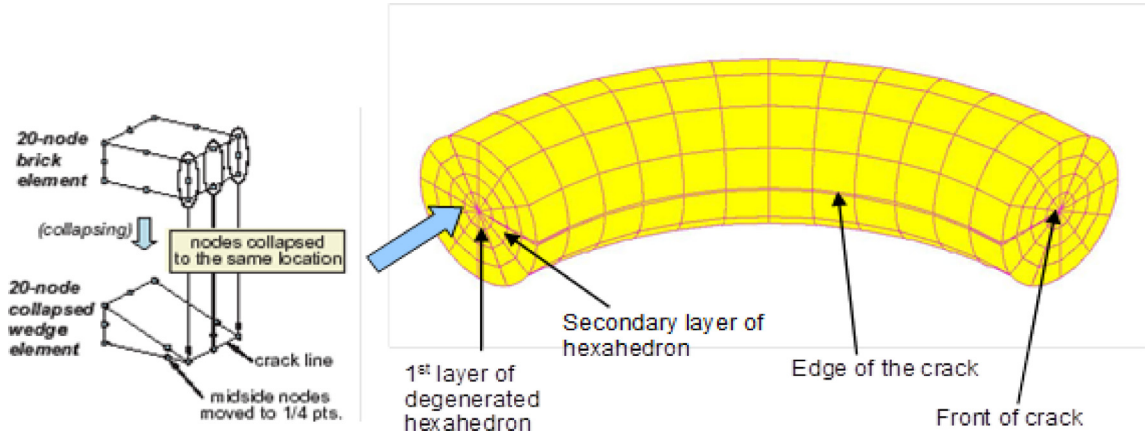

Figure 12 Representation of advanced self-meshing cracking technique.

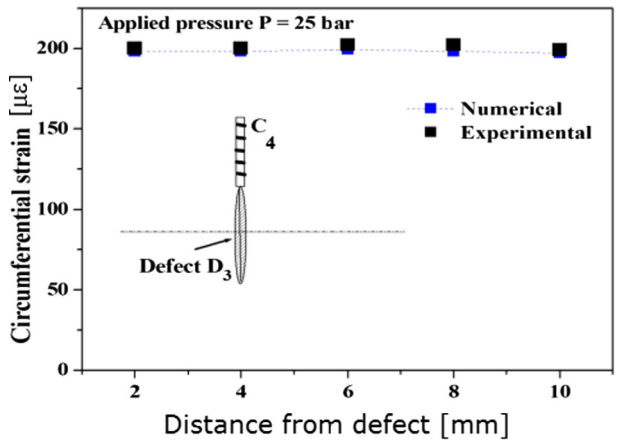

Figure 15 Distribution of circumferential strain near defect D_3.

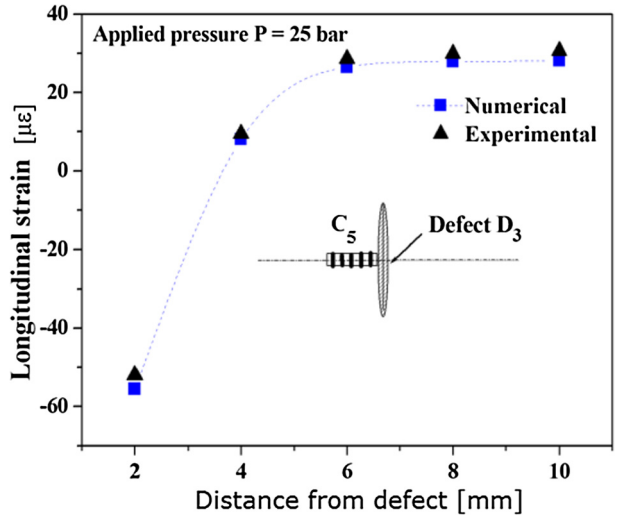

Figure 16 Distribution of longitudinal strain near the defect D_3.

4. Conclusion

This study analysed the structural behaviour of cylindrical shells with external longitudinal and circumferential semi-elliptic defects loaded by internal pressure. The experimental setup employed strain gauges to monitor the evolution of strain field near the defects. A detailed parametric finite element model simulated the experiments. Numerical simulations agreed very well with experimental data (the largest difference on strain values was only 6.2%) and indicated that internally pressurized shells with longitudinal defects are more sensitive to crack propagation than shells with circumferential defects. The numerical/experimental approach developed in this research may concur to simplify design processes, particularly when it is difficult to evaluate the stress/strain field at the tip of three-dimensional cracks.

References

[1] J. Capelle, J. Gilgert, I. Dmytrakh, G. Pluvinage, The effect of hydrogen concentration on fracture of pipeline steels in presence of a notch, Eng. Fail. Anal. 78 (2010) 364–373.
[2] M. Hadj Meliani, Z. Azari, G. Pluvinage, J. Capelle, Gouge assessment for pipes and associated transferability problem, Eng. Fail. Anal. 17 (2010) 1114–1126.
[3] J. Capelle, J. Gilgert, G. Pluvinag, A fatigue initiation parameter for gas pipe steel submitted to hydrogen absorption, Int. J. Hydrogen Energy 35 (2010) 833–884.
[4] G. Pluvinage, M.H. Elwany, Reliability and Risks Assessments with Water, Oil and Gas Pipelines. NATO Science for Peace and Security Series, Springer, 2008, p. 349.
[5] A. Carpinteri, R. Brighenti, S. Vantadori, Notched double-curvature shells with cracks under pulsating internal pressure, Int. J. Press. Vessels Pip. 86 (2009) 1–11.
[6] B.C. Pinheiro, I.P. Pasqualino, Fatigue analysis of damaged steel pipelines under cyclic internal pressure, Int. J. Fatigue 31 (2009) 962–973.
[7] E. Berg, B. Skallerud, C. Thaulow, Two-parameter fracture mechanics and circumferential crack growth in surface cracked pipelines using line-spring elements, Eng. Fract. Mech. 75 (2008) 17–30.
[8] M. Staat, D.V. Khoi, Limit analysis of flaws in pressurized pipes and cylindrical vessels. Part I: axial defects, Eng. Fract. Mech. 74 (2007) 431–450.
[9] M. Kamaya, T. Suzuki, T. Meshii, Failure pressure of straight pipe with wall thinning under internal pressure, Int. J. Press. Vessels Pip. 85 (2008) 628–634.
[10] Y. Lei, J-integral and limit load analysis of semi-elliptical surface cracks in plates under tension, Int. J. Press. Vessels Pip. 81 (2004) 21–30.
[11] ASME B31.8-2012 Gas Transmission and Distribution Piping System.
[12] Staat M, D.V. Khoi, Limit loads of circumferentially flawed pipes and cylindrical vessels under internal pressure, Int. J. Pressure Vessels Pip. 83 (2006) 188–196.
[13] M. Staat, D.V. Duc Khoi, Limit analysis of flaws in pressurized pipes and cylindrical vessels. Part II: circumferential defects, Eng. Fract. Mech. 97 (2013) 314–333.
[14] Y. Lei, A review of limit load solutions for cylinders with axial cracks and development of new solutions, Int. J. Press. Vessels Pip. 85 (2008) 825–850.
[15] Y. Lei, Use of local and global limit load solutions for plates with surface cracks under tension, Int. J. Press. Vessels Pip. 84 (2007) 545–559.
[16] Y. Lei, P.J. Budden, Limit load solutions for plates with embedded cracks under combined tension and bending, Int. J. Pressure Vessels Pip. 81 (2004) 589–597.
[17] Y. Li, Y. Lei, Z. Gao, Global limit load solutions for thick-walled cylinders with circumferential cracks under combined internal pressure, axial force and bending moment e Part I: theoretical solutions, Int. J. Press. Vessels Pip. 114–115 (2014) 23–40.
[18] Z. Gao, G. Cai, G. Liang, Y. Ley, Limit load solutions of thick-walled cylinders with fully circumferential cracks under combined internal pressure and axial tension, Nucl. Eng. Des. 238 (2008) 2155–2164.
[19] Y. Li, Y. Lei, Z. Gao, Global limit load solutions for thick-walled cylinders with circumferential cracks under combined internal pressure, axial force and bending moment Part II: finite element validation, Int. J. Press. Vessels Pip. 114–115 (2014) 41–60.
[20] NF A 03-001, NF EN 10002-1, Essai de traction, Partie: Méthode d'essai (à la température ambiante), AFNOR, 1990.
[21] S. Timoshenko, N. Goodier, Theory of Elasticity, second ed., McGraw-Hill Book Compagney, New York, 1951.
[22] H. Neuber, Theory of stress concentration for shear-strained prismatical bodies with arbitrary non-linear stress-strain law, J. Appl. Mech. 28 (1969) 544–551.
[23] C.C. Chen, H.I. Pan, Collection of papers on fracture of metals, in: C. Chen (Ed.), Metallurgy Industry Press, Bejing, 1985, pp. 119–219.

Please cite this article in press as: H. Moustabchir et al., Experimental/numerical investigation of mechanical behaviour of internally pressurized cylindrical shells with external longitudinal and circumferential semi-elliptical defects, Alexandria Eng. J. (2017), http://dx.doi.org/10.1016/j.aej.2017.05.022

[24] G. Glinka, A. Newport, Universal feature of elastic notch tip stress fields, Int. J. Fract. 9 (1985) 143–150.
[25] Code Français Construction des Appareils à Pression non soumis à l'action de la flamme, édition, 2002.
[26] H. Moustabchir, Z. Azari, S. Hariri, I. Dmytrakh, Experimental and numerical study of stress-strain state of pressurised cylindrical shells with external defects, Eng. Fail. Anal. 17 (2010) 506–514.
[27] H. Moustabchir, C.I. Pruncu, Z. Azari, et al, Int. J. Mech. Mater. Des. 12 (2016) 273, http://dx.doi.org/10.1007/s10999-015-9296-z.
[28] M. Laydi, P. Lesaint, Sur les éléments finis rationnels de Serendip de degré quelconque, Numerische Mathematik June 1985, vol. 46, Issue 2, pp. 175–187.
[29] J.G. Williams, P.D. Ewing, Fracture under complex stress – the angled crack problem, Int. J. Fract. 4 (1972) 416–441.

Please cite this article in press as: H. Moustabchir et al., Experimental/numerical investigation of mechanical behaviour of internally pressurized cylindrical shells with external longitudinal and circumferential semi-elliptical defects, Alexandria Eng. J. (2017), http://dx.doi.org/10.1016/j.aej.2017.05.022